e-Polymers **2004**, no. 067.

http://www.e-polymers.org
ISSN 1618-7229

Molecular deformation mechanisms and mechanical properties of polymers simulated by molecular dynamics

Ricardo Simões [1,2] *, *António M. Cunha* [1], *Witold Brostow* [2]

[1] Department of Polymer Engineering, University of Minho, 4800-058 Guimarães, Portugal; Fax +351 253510339; rsimoes@dep.uminho.pt, amcunha@dep.uminho.pt

[2] Laboratory of Advanced Polymers and Optimized Materials (LAPOM), University of North Texas, Denton, TX 76203-5310, USA; brostow@unt.edu

(Received: July 6, 2004; published: October 22, 2004)

Abstract: Virtual polymeric materials were created and used in computer simulations to study their behavior under uniaxial loads. Both single-phase materials of amorphous chains and two-phase polymer liquid crystals (PLCs) have been simulated using the molecular dynamics method. This analysis enables a better understanding of the molecular deformation mechanisms in these materials. It was confirmed that chain uncoiling and chain slippage occur concurrently in the materials studied following predominantly a mechanism dependent on the spatial arrangement of the chains (such as their orientation). The presence of entanglements between chains constrains the mechanical response of the material. The presence of a rigid second phase dispersed in the flexible amorphous matrix influences the mechanical behavior and properties. The role of this phase in reinforcement is dependent on its concentration and spatial distribution. However, this is achieved with the cost of increased material brittleness, as crack formation and propagation is favored. Results of our simulations are visualized in five animations.

1. Introduction

The deformation mechanisms taking place at the macromolecular level are not yet fully understood. It is generally accepted that a number of different mechanisms occur, depending on the structure of the material and the thermo-mechanical conditions associated to the imposed load. Several models were proposed to explain the specific mechanisms that allow the material to respond to an external load, such as chain uncoiling, chain sliding, crack formation and propagation, and splitting of lamellae in semi-crystalline polymers. However, the conditions and requirements for each mechanism to take place are far from established. To understand and to model those deformation mechanisms are fundamental steps for the prediction of the mechanical properties of polymers.

Computer simulations have been performed with the aim of, among other topics, providing insights into this problem. The present paper reports computational results for simple polymer models under conditions that will enable the identification and study of some of the deformation mechanisms referred above.

Both amorphous polymers and two-phase polymer liquid crystals (PLCs) have been investigated. The latter represent relatively new and insufficiently explored materials.

Unlike traditional purely flexible polymers, PLCs are typically copolymers consisting of rigid liquid crystalline (LC) sequences combined with flexible sequences [1]. Thus, in PLCs there is no lack of adhesion between the flexible constituent and the reinforcement – the main drawback of traditional heterogeneous composites [2,3]. Since the rigid LC constituent is not homogeneously dispersed throughout the material, it is possible that certain spatial arrangements of the second phase within the PLC material provide higher mechanical stability than others when the material is subjected to an applied load.

When compared to other polymers, PLCs exhibit a series of improved properties [4-6]. Due to their complexity, they have been concomitantly studied by statistical mechanics [7,8], viscoelastic models [9-11], and experimental methods [1,4-6]. Previous and ongoing results from computer simulations of PLCs can provide information to complement these other approaches.

As eloquently formulated by Fossey [12], simulations provide information not readily accessible experimentally, either due to the prohibitive nature of the tests, the inadequacy of existing equipment and techniques to study a particular phenomenon, or other impediments. Two very important advantages of computer simulations are the ability to study extreme conditions that cannot be replicated in a controlled environment, and even more important, being able to study the effects of one system variable at a time. In the case of PLCs, an important advantage of computer simulations is the much lower cost compared to extensive laboratory experimentation with these materials. Also, controlling their morphology – the dispersion of the LC phase – is possible but very difficult in experimental methods.

Due to the large amount of data resulting from the simulations, it is of paramount importance to develop adequate means to scavenge that information for pertinent results and to represent those results. For this, it becomes essential to employ 3D visualization and animation techniques that enable real-time observation of the phenomena taking place in the molecular-level simulations.

It is important to point out that these simulations are not performed with the intent of *replacing* experimental testing, but rather to complement it. The concomitant use of computer simulations and experiments should produce a synergistic effect, eventually leading to a more complete understanding of the properties and behavior of polymeric materials.

2. Applications of molecular dynamics to polymer behavior and properties

A detailed review of the various computer simulation methods has been provided by Fossey [12] and will not be covered here. However, some important research efforts conducted on computer simulations shall be briefly mentioned.

In recent years, molecular dynamics (MD) simulations have been used to study a wide variety of phenomena, in many different fields of work. Smith et al. [13] used MD to simulate the X-ray scattering pattern, while Gerde and Marder [14] investigated friction and its connection to the mechanism of self-healing cracks. Theodorou et al. have investigated the phenomena of diffusion [15], permeation [16], elongational flow [17], and stress relaxation [18]. However, they have performed their simulations mostly at the atomistic level, following a different approach from the one employed in the present study.

Other relevant MD applications in materials science include the investigation of the thermodynamic properties of simple fluids and polymer melts [19,20], the melting process, including that of thin layers on a substrate [21,22], and the transport of fluids through a polymer membrane [23]. It is also of interest to mention the kinetic model of fracture, used by Termonia and co-workers to simulate the mechanical behavior of polymers [24-26] and the simulation of spider silk fibers [27], and the use of fracture mechanics in the simulation of polymers [28-31].

In earlier work, computer simulations have been used to study stress relaxation in metals and polymers [32,33]. The presence of defects was found to increase the time span for relaxation, this by several orders of magnitude. These simulations have also indicated that stress relaxation is mainly achieved by plastic deformation occurring in the vicinity of defects. In an ideal lattice, the force required to initiate a crack is higher, but then the force is sufficient to cause quick propagation. The stress-relaxation curves obtained in the simulations have all the essential features of experimental curves and are in accordance with the Kubát cooperative theory of stress relaxation in materials.

The tribological properties of polymeric materials have also been investigated; recently developed scratching simulations are providing information about which structures are most resistant to scratch [34]. These have shown that the local structure affects scratch resistance and recovery, and that the preferential migration of a rigid second phase to the surface of a two-phase material can improve its performance.

The present paper follows previous work on the use of computer simulations to study mechanical properties [35] and crack formation and propagation in polymer liquid crystals (PLCs) [36]. The key question is, obviously, where cracks form in the material and how they propagate. Cracks could have equally been expected to form in the flexible matrix because of its relative weakness or inside the second phase because of its relative rigidity. Simulations have shown that cracks preferentially appear between second phase agglomerates in close proximity and grow next to the interface between the two phases. Cracks can then propagate through the flexible phase, for example in order to connect to another crack.

3. Simulation model

In these simulations, the amorphous chains are represented using the statistical segment model, as advocated by Flory [37]. Here, each segment represents several repeating units of a polymeric chain. The creation of materials on the computer is described in section 4.

The segments interact according to a set of potentials that differ for intra-chain chemical bonding and inter-chain secondary interactions, the later being much weaker. In order to study one- and two-phase systems, different potentials have also been defined to represent the interactions between segments of the flexible polymer matrix and those of a rigid liquid-crystalline (LC) second phase. A narrow Morse-like potential is used for the intra-chain bonds between rigid LC segments, whereas for the intra-chain bonds between flexible segments a spliced double-well potential has been incorporated. This double-well potential allows for conformation transitions as in real polymer chains. The weaker inter-chain (secondary) van der Waals interactions are represented by a Morse-like potential with a relatively broad well. A detailed description of the interaction potentials has been provided in ref. [35].

The simulations have been performed using the molecular dynamics (MD) method, with the time evolution calculated through a leap-frog algorithm [38]. The preference over the Monte Carlo (MC) or Brownian dynamics methods has been previously discussed [35,36]. The MD method was developed by Alder and Wainwright, with the initial intent of studying the phase diagram of a system of hard spheres [39]. Later, continuous potentials have been introduced to provide a more accurate representation of the forces acting on each particle in the system. Soon after that, Rahman implemented Lennard-Jones potentials in his simulations [40], creating the foundation for most of the work being currently done in this area.

In the MD method, a system of N particles (statistical segments in this case) is considered, each of them characterized by three Cartesian coordinates and three momentum components along the main axes. These variables are calculated at each time step of the simulation, effectively describing the time-dependent behavior of every segment in the system. In contrast to traditional MC in which one particle moves at a time, here all particles are moved at once at each time step. Since time is an explicit variable in MD, the method can be used to simulate not only equilibrium properties but also time-dependent ones. This is particularly important when dealing with viscoelastic materials.

The segments are disturbed from their initial lattice-based positions by a small fraction of the average intersegmental distance before the simulation begins. During the first stage of the simulation, the material is allowed to equilibrate for a few thousands of time steps without any external forces applied. After a quasi-equilibrium state has been reached, a uniaxial external tensile force is applied to the edges of the material along the x-axis and the state of the system is monitored and periodically recorded. The value of the external force continuously increases until fracture is observed.

The employed MD simulation method assumes that the forces on particles are nearly constant over very short periods, which defines the time step for the simulation. It can be shown that in the limit of short time steps, this procedure samples states accessible in the micro-canonical ensemble. However, additional features can be added to the algorithm that allow one to specify the configurational temperature, or allow the simulation to access a range of energies and/or pressures that correspond to either the canonical or isothermal-isobaric ensembles.

When using the micro-canonical ensemble, one maintains the number of particles, volume and energy (NVE) constant throughout the simulation. However, the simulations reported in this paper were performed at constant temperature, to avoid an effect of stochastic thermal forces, since the purpose is to study non-thermal sources of polymer fracture [32]. Also, the material is allowed to deform freely along all three axes. This implies that upon sufficient deformation, there is formation and propagation of cracks, which contributes to an increase of the internal free volume. Thus, this procedure is closer to the isothermal ensemble. When performing constant-temperature MD [38], one has to rescale the velocities at each time step, based on the kinetic energy of the system. Further details concerning the simulation model were provided in ref. [35] and in the Appendix.

4. Material generation procedures

For these simulations, both one- and two-phase polymeric materials were created on the computer. In both cases, the matrix consists of amorphous chains with a

molecular weight distribution. For the two-phase systems, a rigid liquid-crystalline (LC) phase is then dispersed in the flexible matrix. After the material is generated and before the simulation begins, columns of rigid segments are placed at the left and right edges of the material, in order to avoid chain pullout; see for example Animation 2. The external force is applied to these segments and they transfer it to the bulk material. These rigid edges can be considered the simulation equivalent of the opposing clamps in a tensile test apparatus.

4.1. Two- and three-dimensional structures of amorphous chains

The amorphous phase is created using an approach developed by Mom [41] and later modified to suit specific needs [42]. Initially, all segments in the material are positioned in equidistant lattice positions, each segment representing at this stage one chain of length 1. The triangular lattice has been chosen for several reasons stated before [42]. Particularly, this lattice results in a more realistic coordination number than, for example, the square lattice. This methodology is effective both for completely filled lattices and those containing vacancies.

After the segments are placed, the system is searched for neighboring end-of-chain segments. At the first stage, all segments fulfill this condition and, therefore, a statistical function determines which segments bond together forming chains of length 2. The chains continue to grow by bonding of adjacent end-of-chain segments until no more segments can be bonded in this way. When a segment can equally bond to several others, the preferential direction of the bonding can be statistically controlled in order to give rise to structures with varying degrees of orientation. However, in the present work only the two limiting cases were investigated: structures completely aligned with a specific direction and structures with no preferential orientation. Although this is a simple procedure, the resulting computer-generated materials (CGMs) exhibit realistic features, such as a molecular weight distribution and physical entanglements between chains [42].

4.2. Second phase incorporation and distribution

A rigid LC second phase can be added to the flexible matrix to mimic the structure of polymer liquid crystals (PLCs). In these materials, the LC phase has been experimentally found to form quasi-spherical agglomerates, often designed by *islands* [43]. Islands are introduced in the CGMs by random sequential addition, until the desired concentration is achieved. The random placement of the islands sometimes results in regions of high local concentration, which was found to greatly affect crack initiation and crack propagation [35]. The present paper addresses the influence of the LC phase concentration on the mechanical properties, as well as the behavior of specific spatial distributions of the islands. For the latter, hand-made CGMs have been created where the islands are placed at desired locations.

A more detailed description of the entire one- and two-phase material generation procedure, including a brief review of alternative methods to generate polymeric materials on a computer, has been provided in ref. [42].

5. Selected results

In section 5.1 results are described pertaining to a single-phase CGM contained within a simulation cell with approximately 1500 statistical segments, as well as a

two-phase CGM of the same dimensions containing 25% LC phase. These two materials were created on a two-dimensional lattice and are both comprised of macromolecular chains oriented with the direction of force application.

Results for a single-phase CGM created on a three-dimensional lattice are discussed in section 5.2. In the three-dimensional CGMs, chains are allowed to grow with no preferential orientation, following the procedure described in section 4.1, leading to structures of coiled macromolecular chains with a molecular weight distribution. Because of this, a larger number of deformation mechanisms can take place. The presence of entanglements between chains in three-dimensional materials and their effect on the mechanical behavior is described in section 5.3. The effect of the concentration and distribution of the rigid second phase on the material behavior and properties is discussed in sections 5.4 and 5.5. The influence of the LC island size was also studied and is covered in section 5.6.

5.1. Deformation mechanisms in two dimensions (2D)

A structure of aligned chains is used in the simulations to represent highly oriented polymer liquid crystals, where each row of segments constitutes a single chain (see Animation 1). High degree of orientation of PLCs under magnetic fields has been previously reported [44]. However, it is important to remember that results from 2D simulations are not comparable to 3D reality, among other reasons, for the lack of many features of real materials in a 2D model.

For these materials, since chains are initially already uncoiled and no entanglements exist, the only mechanism that allows chain extension is the conformation change of flexible bonds. For large-scale deformation, rupture of bonds will have to occur at high force levels. The different stages of the simulation of the purely flexible material are shown in Animation 1. In this animation, as well as Animations 2, 4 and 5, a specific color code was used. Flexible segments are represented as empty spheres and rigid segments as dark spheres. Rigid segments belonging to islands are drawn in black, whereas those comprising the rigid edges are drawn in gray. Whenever a bond has been broken, the respective segments are drawn in blue (for flexible segments) or red (for rigid segments).

Animation 1	Animation 2	Animation 3	Animation 4	Animation 5
3.2 MB	1.9 MB	7.0 MB	1.9 MB	3.1 MB

Click here on ‘Animation *x*’ to view it.

As previously mentioned, the force increases at a constant rate from the value of zero in the beginning of the simulation until fracture is observed. At every force step, which corresponds to 2000 time steps, a snapshot of the status of the material is taken and the value of the force is updated. In this paper, the force step is designated by *t*, and indicates the progress of the simulation along time.

Deformation for the first 11 force steps is negligible, since the force level is too low for the bonds to cross the energy barrier required for short to long conformation change. The first noticeable conformation changes occur at $t = 12$. From this point on, deformation increases significantly. At $t = 25$, most bonds have already changed conformation except for a small region near the center of the material. All simulations

performed exhibit this effect; bond conformation changes start at the edges of the material and move towards the center. As the deformation process is far from an equilibrium process, this is not surprising.

Since the force is applied at the edges, it must be transferred from segment to segment. That process is not instantaneous, and if the force is sufficient to cause a change in conformation near the end of the chain, the resulting increase in bond length may accommodate for the present loading conditions and halt the process. Thus, at any given time, it is more likely to find short bonds near the center. However, this is significantly affected by the presence of a second phase, as discussed below and in ref. [35].

All bonds have already changed conformation around t = 32. At this stage, the material remains practically unchanged until t = 47. Since all bonds have changed to the long conformation, there are no other mechanisms available for deformation of the material. The force has to increase substantially until it is high enough to break primary bonds, which occurs at t = 47. More broken bonds appear at t = 52 and the number of broken bonds continues to increase at every force step. At t = 79 the majority of the bonds have been broken throughout the material, yet no large cracks can be observed. The first cracks appear in several locations simultaneously at t = 80. These cracks continue to grow until the material fractures.

The purely flexible material exhibits a random and homogeneous distribution of conformation changes and broken bonds during deformation. This is reasonable, since all segments in the material are equal. However, the situation changes when a liquid crystalline (LC) second phase is added to the flexible matrix. The different stages of the simulation of the 25% LC material are shown in Animation 2.

Similarly to the flexible material, deformation is negligible for several force steps. At t = 10, the first bond conformation changes are observed. In the subsequent force steps, bonds continue to change conformation. However, in the case of the two-phase material, the first broken bonds appear at t = 18 with most flexible bonds still in the short conformation. The presence of the rigid LC islands induces this effect, as discussed in ref. [35].

At t = 25, several bonds have been broken but there are still a few bonds in the short conformation. Small cracks can be identified in different *loci* at t = 30. At this stage, although most bonds have gone through a conformation change, some can still be found in the short conformation. The cracks grow as more bonds continue to break. However, unlike the flexible material, it is possible to clearly distinguish regions where a crack developed and regions that have a low number of broken bonds. This effect is quite noticeable at t = 45. Thus, the presence of the islands influences crack formation and propagation.

Since all segments are equal in the purely flexible material, cracks could be expected to appear anywhere in the material and propagate randomly. However, this is *not* the case of two-phase materials. In these, the morphology will determine where and when cracks will first appear as well as how they propagate through the material. The morphology can be characterized in terms of second phase concentration and distribution, in order to predict crack formation *loci* and crack propagation patterns [36].

The visual interpretation of Animation 1 and Animation 2 in terms of bond conformation changes during deformation can be confirmed by measuring the number of bonds in each state during the simulation. The fraction of flexible bonds in the long conformation state, f_c, is shown in Fig. 1.

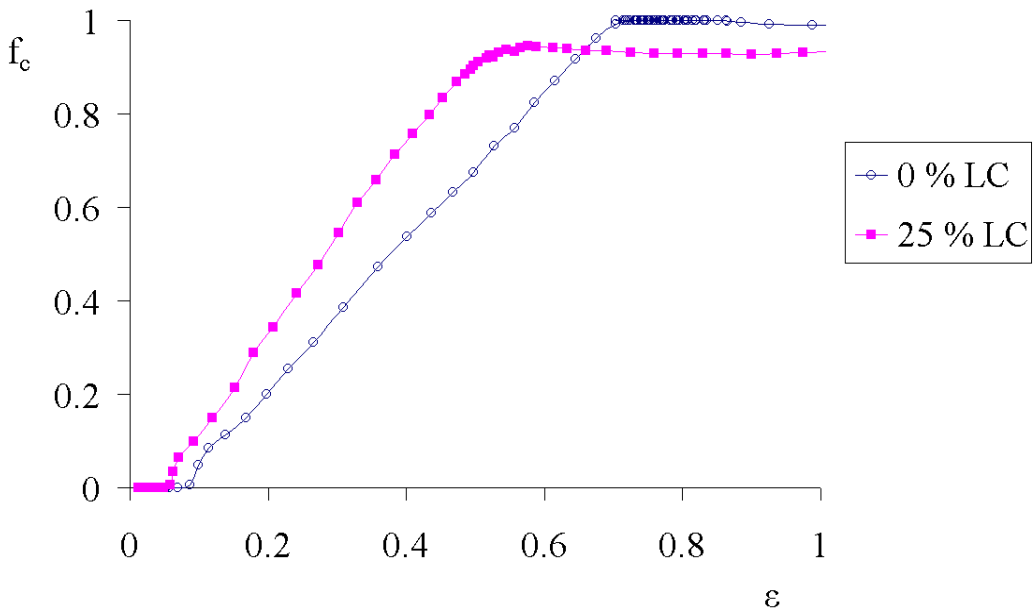

Fig. 1. Bond conformation changes during deformation for the one- and two-phase materials. Here, f_c is the fraction of flexible bonds in the long conformation state and ε is the strain

The purely flexible material shows an almost linear increase of long bonds up to a point where all bonds have changed conformation at high strain values. After that point, further deformation can only be achieved through bond rupture. The 25% LC material also exhibits linear increase of long bonds but with a higher slope, which implies that conformational changes are occurring sooner during the simulation. These materials never reach a state where all bonds have changed conformation. Furthermore, the maximum f_c is reached at lower strain values than in the case of the purely flexible material, which is due to LC islands limiting the conformation changes in their vicinity. Instead, bond rupture and crack growth enable deformation without further conformation changes.

5.2. Deformation mechanisms in three dimensions (3D)

Several mechanisms developing in systems of coiled chains created in three dimensions (3D) were not possible for aligned chains in 2D. First, the geometry of the chains allows chains to uncoil and orient themselves with the applied force. Also, since each chain in the material has a different length and the force is not applied directly to end-of-chain segments, chain separation can occur, for example through a sliding mechanism. These two phenomena take place even at low force values, since it only requires breaking weak intermolecular forces. Last, chains can be entangled in 3D materials, thus creating physical connection points. Depending on the extension of the entanglement between two chains and their particular geometry, motion of those chains in opposite directions might be equivalent to a cross-link point and thus require rupture of primary bonds.

In addition to these mechanisms of deformation, the mechanisms that were presented in section 5.1 for materials of oriented chains can also take place in 3D materials of coiled chains. Besides rupture of primary bonds, flexible bonds can undergo bond conformation changes at relatively low values of the force. Thus, these materials exhibit competing deformation mechanisms, dependent on the structure of

the material and loading conditions. The chain separation mechanism can be easily demonstrated to occur during the deformation of coiled chains. For ease of visualization, a 2D material is considered, as shown in Fig. 2. It is easy to verify the presence of chain separation in this simple material structure due to its small number of chains. In larger materials, chain separation would occur in several locations simultaneously but would be difficult to identify and study.

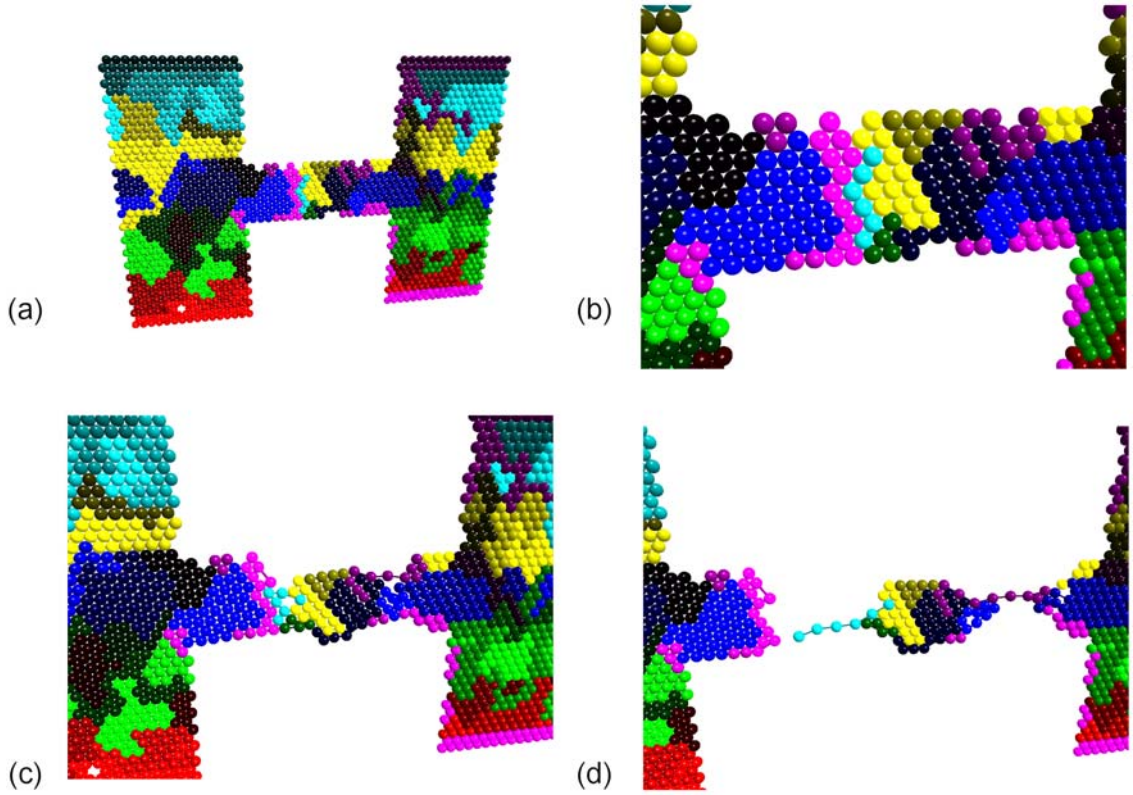

Fig. 2. Deformation through chain separation: a) initial material structure; b) a detailed view of the region where deformation will occur; c) two deformation loci appear at an early simulation stage; d) complete chain separation resulting in material fracture

In order to demonstrate the existence of chain uncoiling during deformation, the evolution of specific chains can be followed, now in a 3D material; see Fig. 3a and b. At an intermediate stage of the simulation, as shown in Fig. 3c, the two chains that extend through the material have suffered significant deformation, mostly through uncoiling but also some bond conformation changes. The bonds that changed conformation are indicated by arrows. The rightmost chain remains nearly unchanged, since it is part of the edge of the material and in this case, deformation is taking place in the inner region.

The geometry of the chains after several additional force steps is shown in Fig. 3d. The topmost chain has uncoiled and extended, becoming more orientated with the direction of force application, although the number of long bonds remains the same. The bottom chain has been ruptured, and each part of that chain is now moving in opposite directions. Rupture occurred without complete bond conformation changes in this chain, due to the influence of neighboring chains. The rightmost chain still exhibits only minor geometry changes.

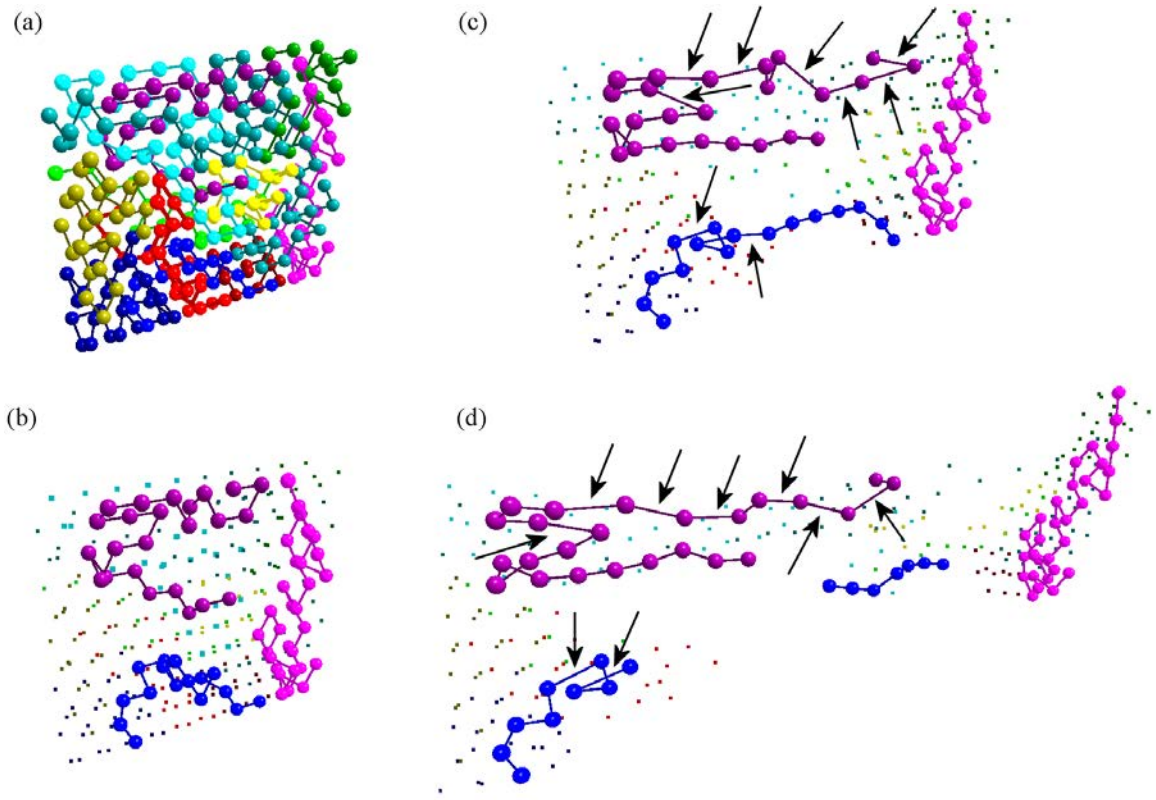

Fig. 3. Deformation through chain uncoiling: (a) structure of the material before deformation; (b) initial geometry of selected chains; (c) geometry of the selected chains at an intermediate simulation stage; (d) geometry of the selected chains near fracture. In (b), (c) and (d), segments not belonging to the three chains being studied are represented only by dots for clarity

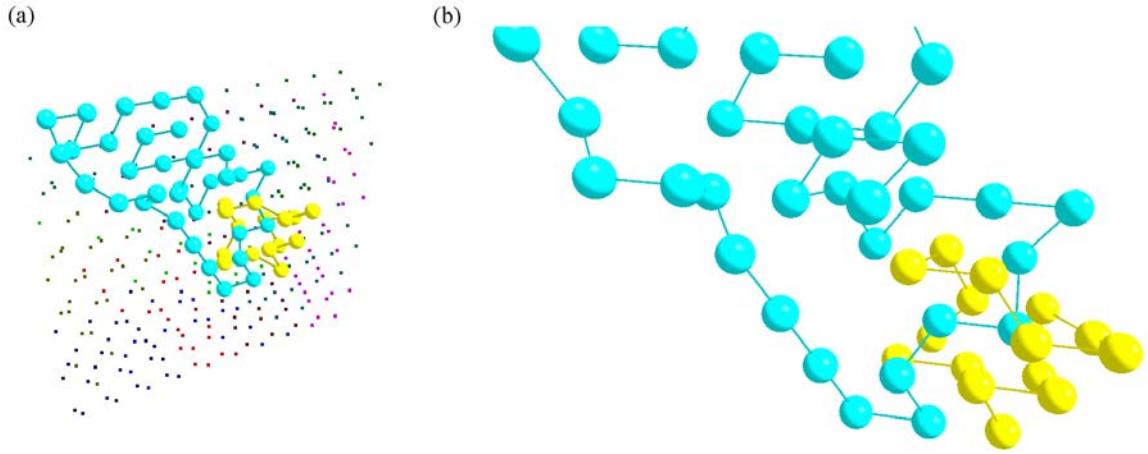

Fig. 4. Chain entanglements in 3D materials of coiled chains: a) two entangled chains; b) a detailed view of the entanglement. Only the two entangled chains are fully represented

5.3. Chain entanglements

The presence of entanglements in 3D materials of coiled chains is an important feature and can be graphically verified. The effect of molecular entanglement density on the mechanical behavior of polymers has been reported by Seguela and Rietsch

[45]. The material previously represented in Fig. 3 has two entangled chains, as shown in Fig. 4.

The influence of this entanglement on the deformation of the material during the simulation is shown in Animation 3. Fig. 5 represents different stages of the deformation process, evidencing the influence of this entanglement in the interaction between the two chains.

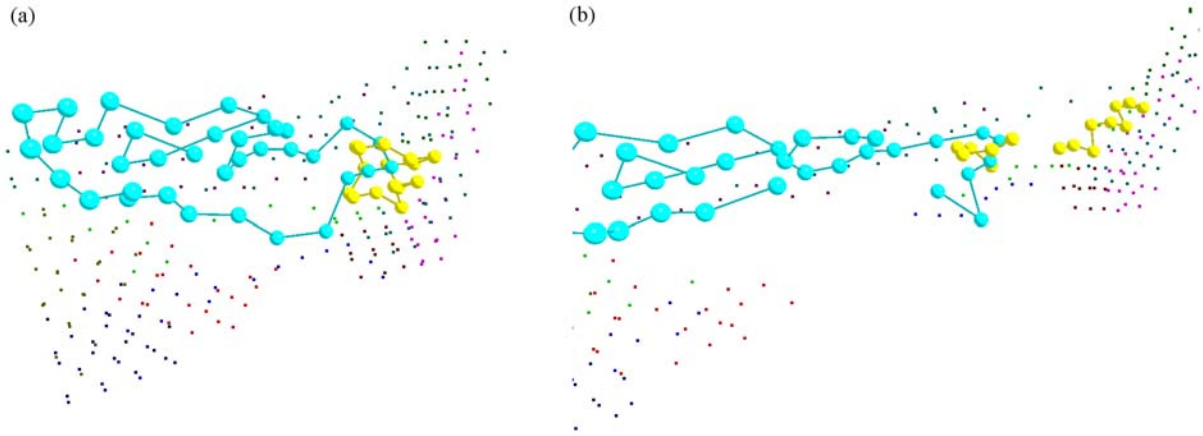

Fig. 5. Effect of chain entanglements on the behavior under tensile deformation: (a) intermediate stage of the simulation; (b) rupture of the entanglement preceding material fracture. All segments in the material not belonging to the two entangled chains are represented only by dots for clarity

The two entangled chains undergo partial uncoiling and re-orientation with the external force, together with bond conformation changes, to allow chain extension. After a certain amount of deformation, the entanglement forces one of the chains to extend and eventually rupture to allow further material deformation. At this point, a piece of the ruptured chain is separated from the rest of it, being displaced along with the other chain due to the entanglement; see again Animation 3.

5.4. Second phase concentration

As previously discussed, the presence and distribution of the LC islands is expected to greatly influence the mechanical properties and behavior of the material. In fact, formation of islands was an important factor in developing a theory of hierarchical structures in PLCs [46].

CGMs were created with varying amounts of the LC phase, up to 35% LC concentration. The structure of all simulated CGMs is represented in Fig. 6. Due to the random placement of islands, higher values become very difficult to obtain. These simulations have been performed with a force increasing at constant rate from zero until fracture was observed. The fracture criteria defined for these simulations was a strain equal to one, which means a length of the material along the *x*-axis of twice the initial length.

The evolution of f_c during deformation is shown in Fig. 7. As discussed in section 5.1, the LC islands induce a decrease in the maximum number of bonds undergoing conformation changes. Simultaneously, that maximum occurs for lower strain values.

The stress-strain curves for the materials with varying LC concentration are shown in Fig. 8. The stress here was represented by the force, since the cross-sectional area in 2D simulations is an ambiguous concept and the calculation of the actual engineering stress would merely change the scale of the graph.

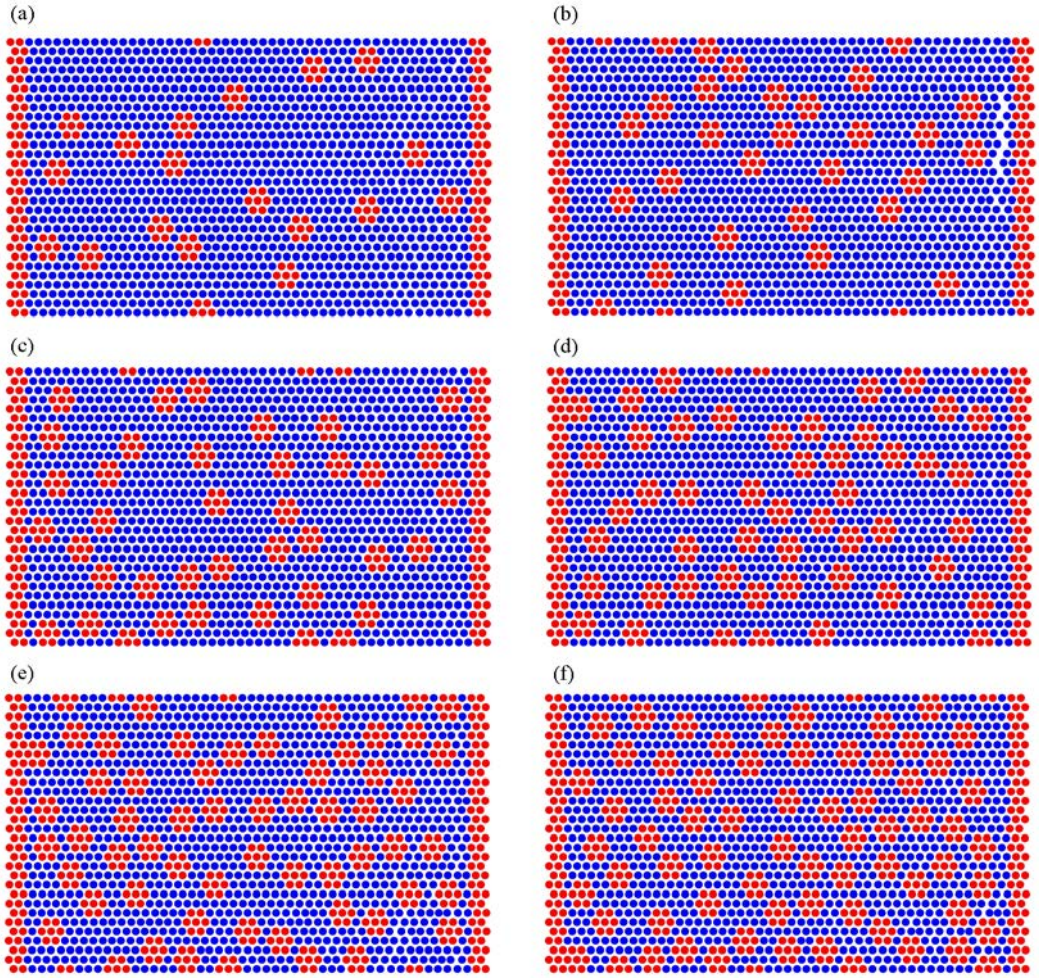

Fig. 6. Two-phase CGMs of island diameter of 3 with varying LC concentration: (a) 10%; (b) 15%; (c) 20%; (d) 25%; (e) 30%; (f) 35%. Flexible segments are represented in blue and rigid segments in red

There are four identifiable regions in the stress-strain curves, marked as R1 through R4 in Fig. 8. The first region is characterized by small increases in strain and corresponds to force levels below the minimum to cause conformation changes. The second region develops over an extended strain range and corresponds to the changes from short to long bond conformation. After all conformation changes have occurred, the curve again shifts to a high slope, with very small increase of strain for several simulation steps. This region lasts until the force is sufficient to break primary bonds. At that point, strain starts increasing significantly again, now due to crack formation and propagation. This last region exhibits a slope similar to the second region.

The increase of LC concentration causes changes in the curves similar to those described for f_c. The slope of the curves tends to increase with increasing concentration, and the points defining the end of R2 and the start of the R4 occur for lower

strains. Thus, the second phase makes the material stronger but simultaneously more brittle. The modulus for each LC concentration is shown in Fig. 9.

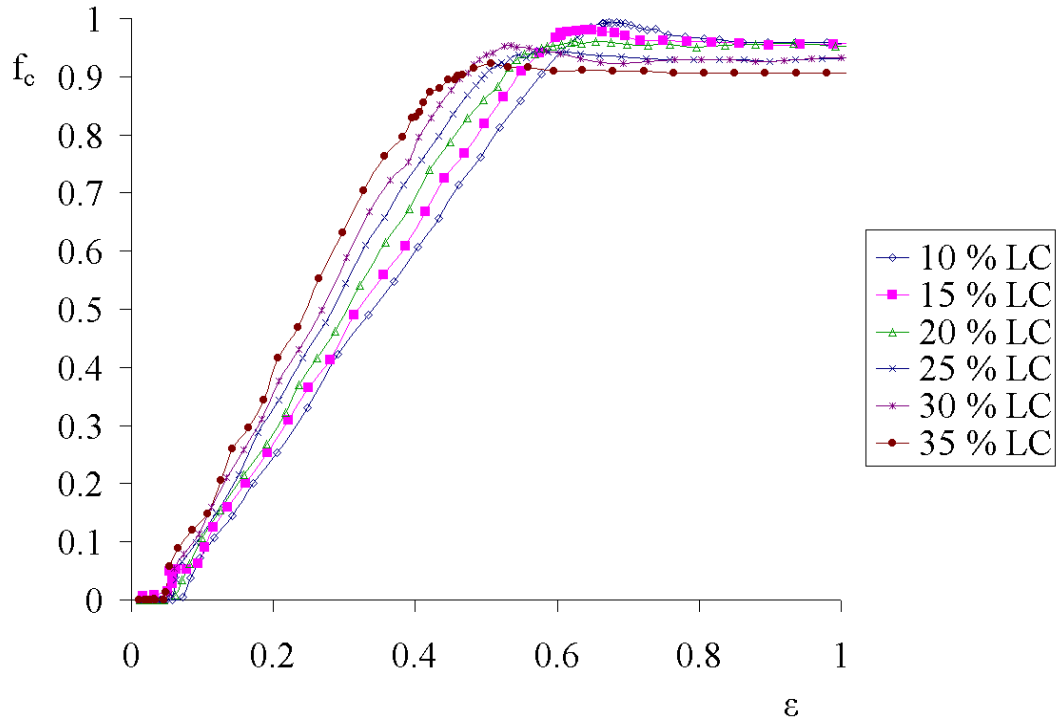

Fig. 7. Effect of the LC concentration on the bond conformation changes. Here, f_c is the fraction of flexible bonds in the long conformation state and ε is the strain

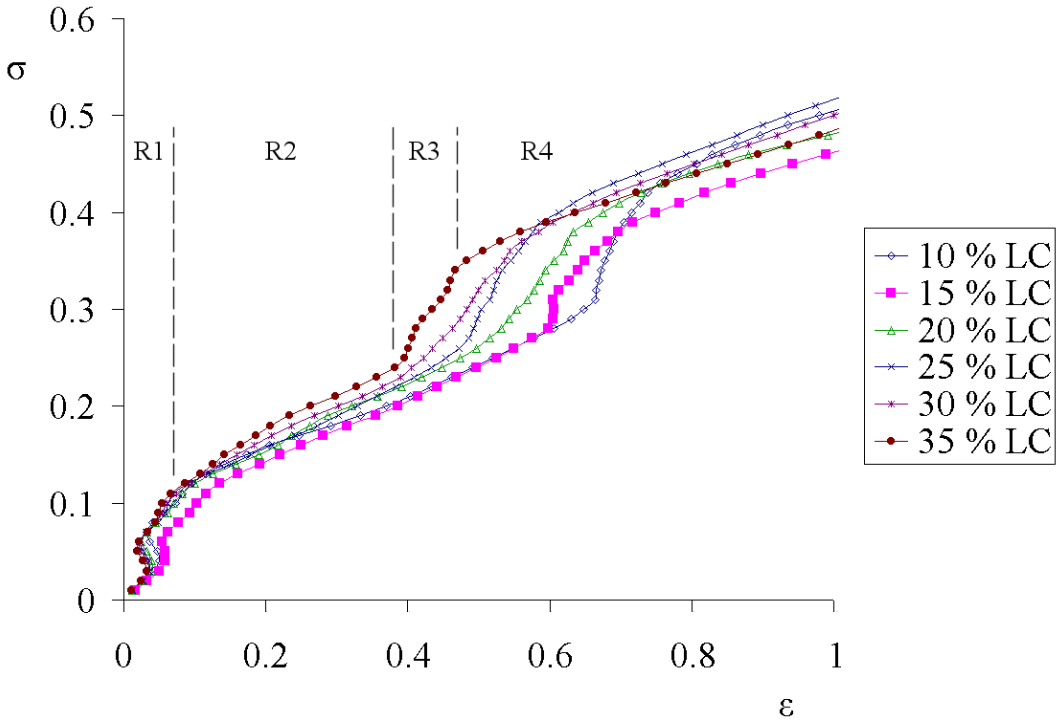

Fig. 8. Stress (σ) vs. strain (ε) curves for materials with varying amounts of the LC phase. R1 through R4 correspond to the four identifiable regions in the curves, exemplified here for the 35% LC material

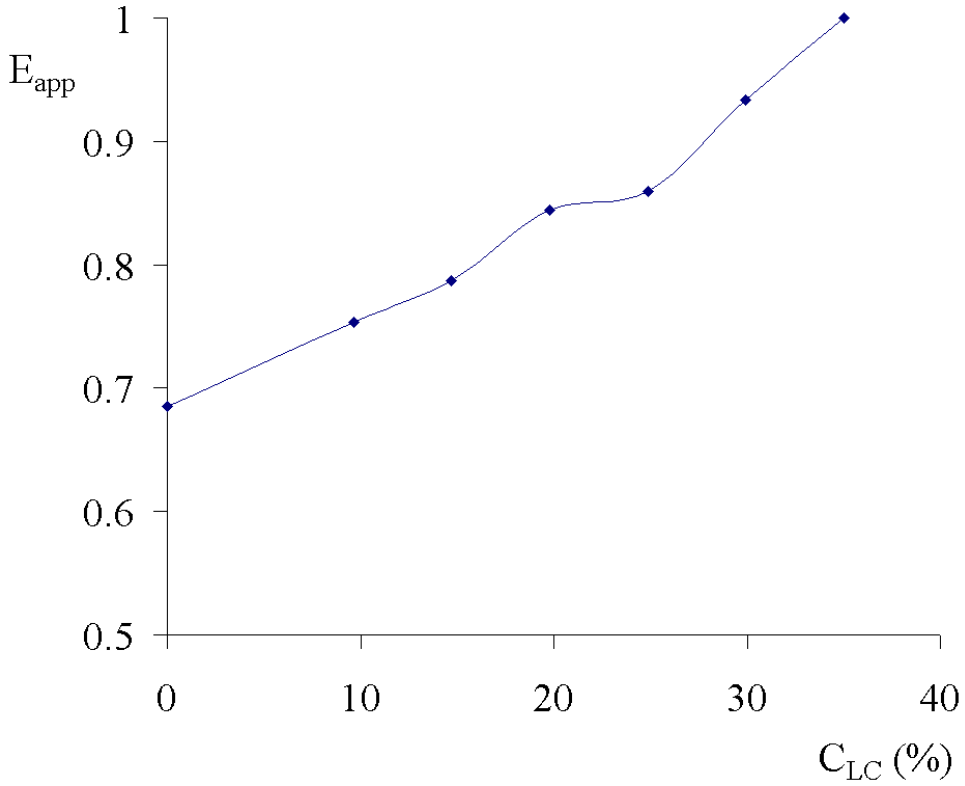

Fig. 9. Effect of the LC concentration (C_{LC}) on the apparent modulus (E_{app}) of the material

The influence of the LC concentration was also investigated for CGMs with varying island size, or island diameter. As discussed in detail in section 5.6, the effects of the second phase concentration on materials with islands of Ø 5 and Ø 7 are similar to those described in the present section for islands of Ø 3.

5.5. Second phase distribution

The simulations discussed so far were performed either on one-phase materials or on two-phase materials containing randomly dispersed LC islands. The random distribution of islands influences the properties of the material. Therefore, not only the overall LC concentration but also its distribution is an important factor to consider.

The influence of the random dispersion of islands in the flexible matrix was discussed in ref. [36]. Now, the behavior of 'hand-made' materials with a patterned island spatial distribution, designated HM1 and HM2, was also investigated. The structure of HM1 and HM2 and the different stages of their simulations are, respectively, represented in Animation 4 and Animation 5.

The configuration of the material with aligned islands (HM1) is characterized by a short distance between neighboring islands along the direction of force application for this particular LC concentration. In contrast, the material with distributed islands (HM2) corresponds to the maximum possible inter-island distance along the direction of force application. Obviously, these materials are ideal cases and not expected to represent a real case, but investigating their properties is nonetheless of interest.

The behavior of f_c during deformation is comparatively shown in Fig. 10. Although the evolution of bond conformation changes is identical for all curves in the linear region,

the curves become different in the region where bonds start to break. The molecular deformation behavior of these two materials is also significantly different.

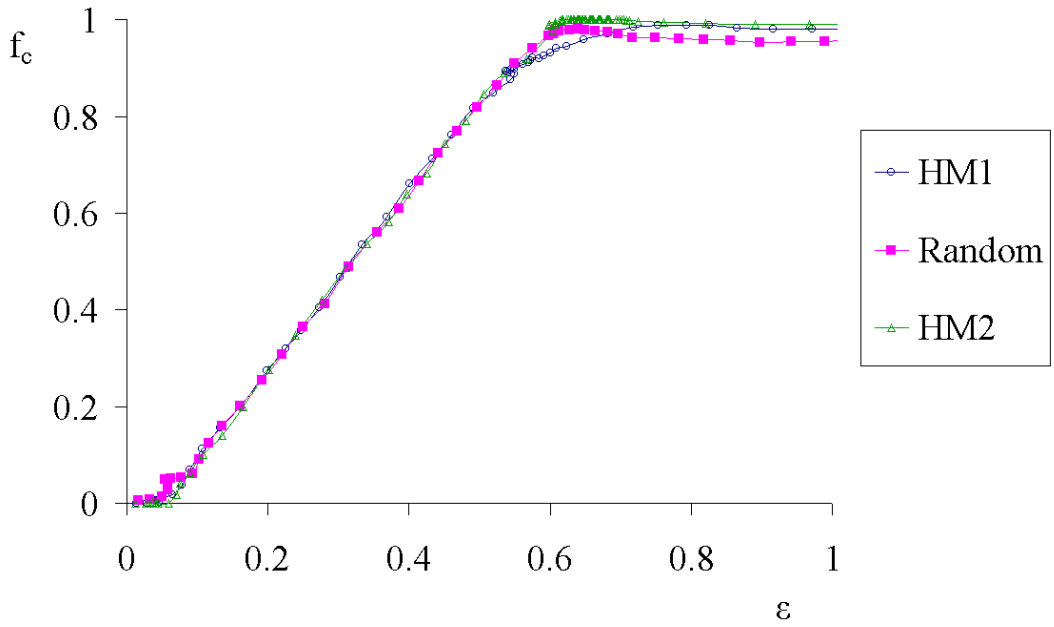

Fig. 10. Bond conformation changes during deformation of random and ordered distributions of the LC islands in two-phase materials. Here, f_c is the fraction of flexible bonds in the long conformation state and ε is the strain

The first conformation changes occur in material HM1 at t = 9 and in HM2 at t = 11. Some isolated broken bonds appear in both materials around t = 23 for HM1 and t = 25 for HM2. However, deformation through bond conformation changes is the main deformation mechanism for several force steps. A significant number of broken bonds n_b is only observed around t = 27 in HM1 and around t = 55 in HM2. At this stage, there are still many bonds in the short conformation in HM1. This effect is also evident in the different shape of the curves for strain values between 0.5 and 0.7; see again Fig. 10. An important aspect observed in the simulations of CGMs of oriented chains is that bond conformation changes occur from the edges towards the center of the material.

Notice that the first broken bonds in HM1 appear in the chains containing islands and *not* in the purely flexible chains. As the simulation continues, n_b increases rapidly in HM1, while in HM2 only a few bonds break at each force step. Moreover, broken bonds are distributed homogeneously in HM2 and more localized in HM1.

For several force steps n_b continues to increase, until the first small cracks develop at t = 41 in HM1 and t = 76 in HM2. At this point, HM2 has many more broken bonds, and is subject to *almost twice* the force level of HM1.

From the moment cracks appear in the two materials, the simulation lasts only a few more force steps. Fracture occurs at t = 49 in HM1 and t = 79 in HM2. Notice how HM1 exhibits several significant cracks throughout the material, while in HM2 only one large crack has propagated. The behavior along time is quite different for HM1 and HM2. Although most phenomena occur in HM1 before HM2, the time span from crack formation to failure is actually lower in HM2 due to the large number of broken bonds.

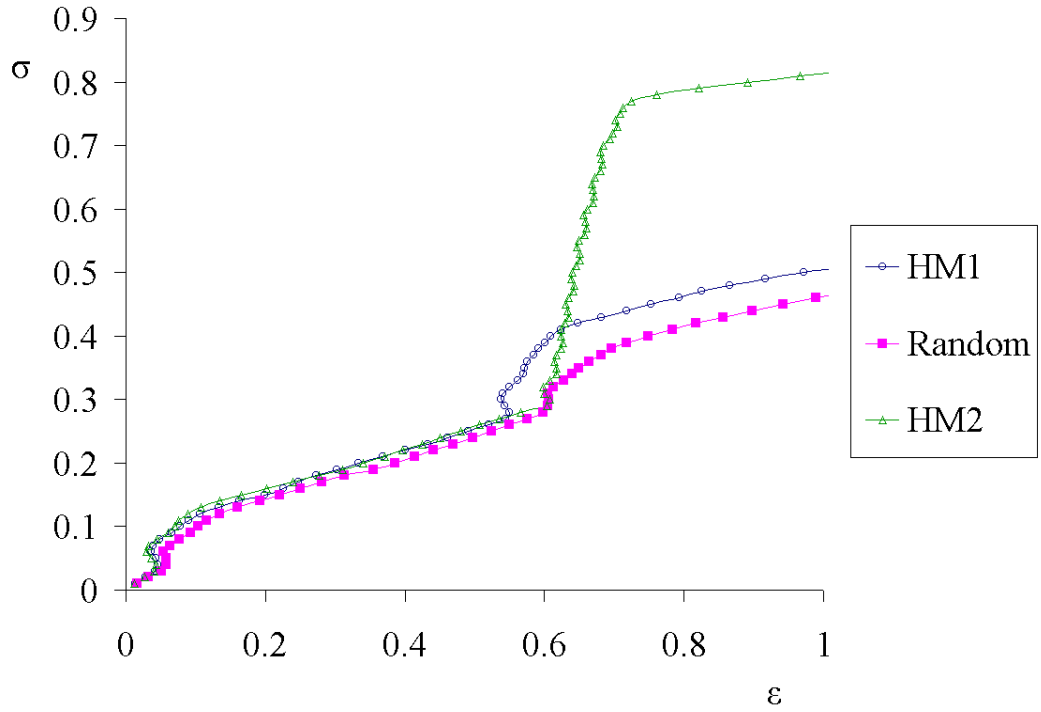

Fig. 11. Stress (σ) vs. strain (ε) curves for materials with random and ordered distributions of the LC islands

The stress-strain behavior of these materials is shown in Fig. 11. The slope of each of the four previously defined regions is similar for HM1 and the random distribution. However, there are significant differences in the case of HM2. This material requires a much higher value of the force for fracture. This is due to the absence of preferential crack formation *loci*, as discussed in more detail in ref. [36]. In contrast, the random distribution favors crack formation. Since force increases at constant rate in these simulations, it is proportional to time. Thus, HM2 resists much longer to failure.

5.6. Effect of the liquid-crystalline (LC) island size

Two-phase materials were created with similar overall LC concentration but varying island size. The size of an island can be characterized by its diameter Ø since they are quasi-spherical. Materials containing islands with Ø 3, Ø 5 and Ø 7 were simulated and the influence of the size of the LC islands on the mechanical properties was investigated. For each island diameter, simulations were performed varying the LC concentration between 10% and 35% in intervals of 5%; see Fig. 6 and Fig. 12 for examples. The size of the islands in real material was found to depend on the concentration of the LC phase [47]. As the second phase concentration increases, the distribution of island sizes also becomes wider.

The stress-strain curves for CGMs with varying island size and 10% overall LC concentration are shown in Fig. 13. As before, the values of the external force were used as a quantitative equivalent to the engineering stress.

The curves are similar in the linear range up to the point where the slope changes at high strain values, where primary bonds start to break and large-scale yielding begins. That is due to larger islands resulting in fewer but larger cracks. The evolution of f_c with deformation can also be compared; this is shown in Fig. 14 for three values of LC concentration with varying island size.

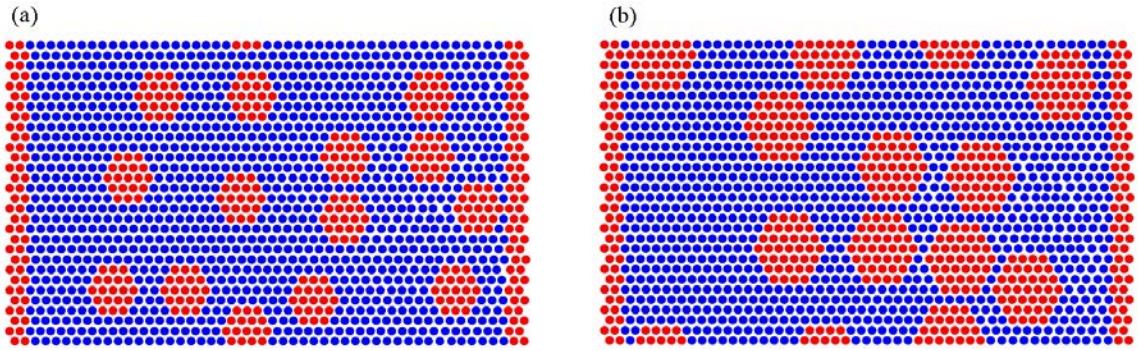

Fig. 12. Two-phase CGMs of varying island diameter and LC concentration: (a) Ø 5, 20%; (b) Ø 7, 30%. Flexible segments are represented in blue and rigid segments in red

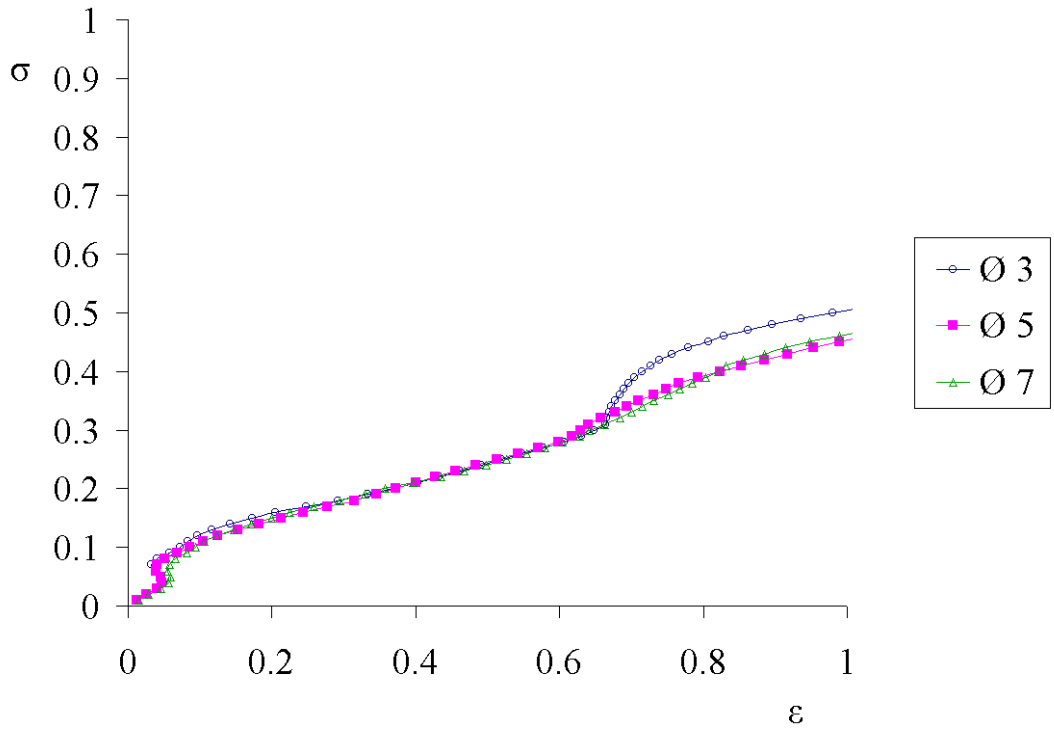

Fig. 13. Stress (σ) vs. strain (ε) curves for two-phase CGMs with varying island diameter

Generally, the curves have the same shape for different Ø. In fact, curves for different Ø at constant LC concentration overlap extensively. The maximum number of bonds that have undergone conformation change before bonds start to break decreases with increased island size, but that effect is weaker than the effect of the LC concentration.

The similarity of the stress-strain curves in Fig. 13 is reflected on the modulus of the material. This is shown in Fig. 15 for different LC concentrations.

The curves in Fig. 15 clearly show that there is only an insignificant dependence on the island size. The curves are shifted higher for increasing LC concentration, as would be expected from the discussion in section 5.4. Since the distribution of the islands changes for each material of different Ø, some of the differences in the behavior at high strain levels cannot be directly attributed to the size of the islands.

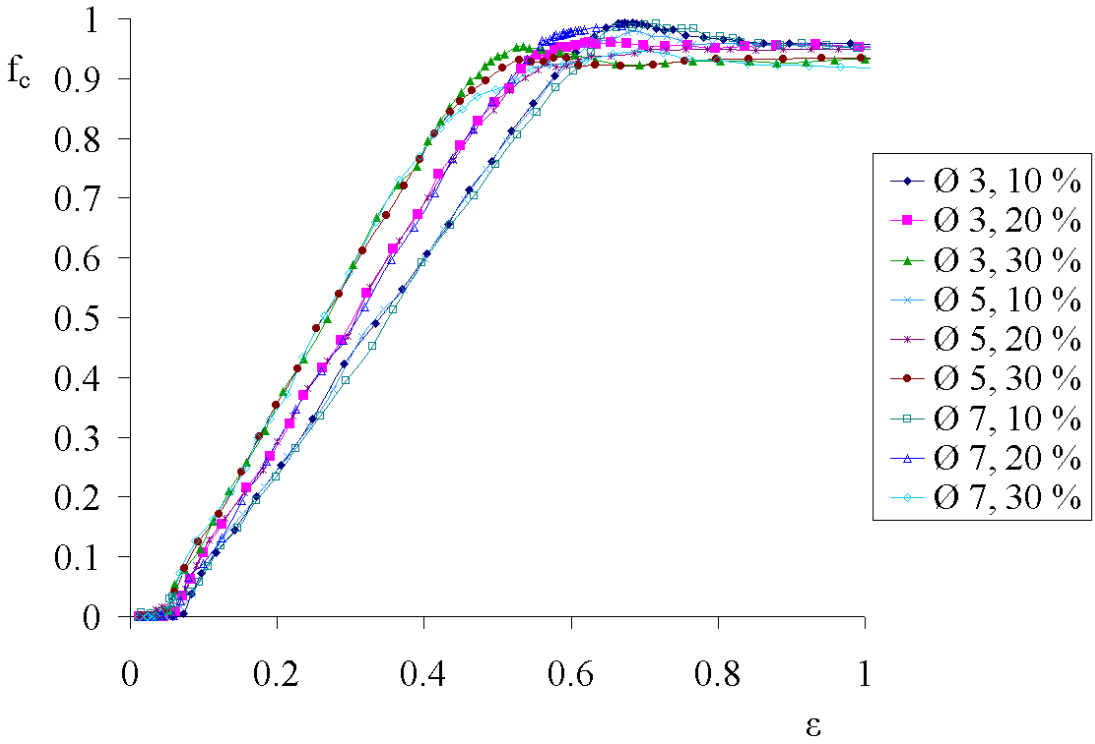

Fig. 14. Evolution of the bond conformation changes in two-phase CGMs with varying LC concentration and island diameter. Here, f_c is the fraction of flexible bonds in the long conformation state and ε is the strain

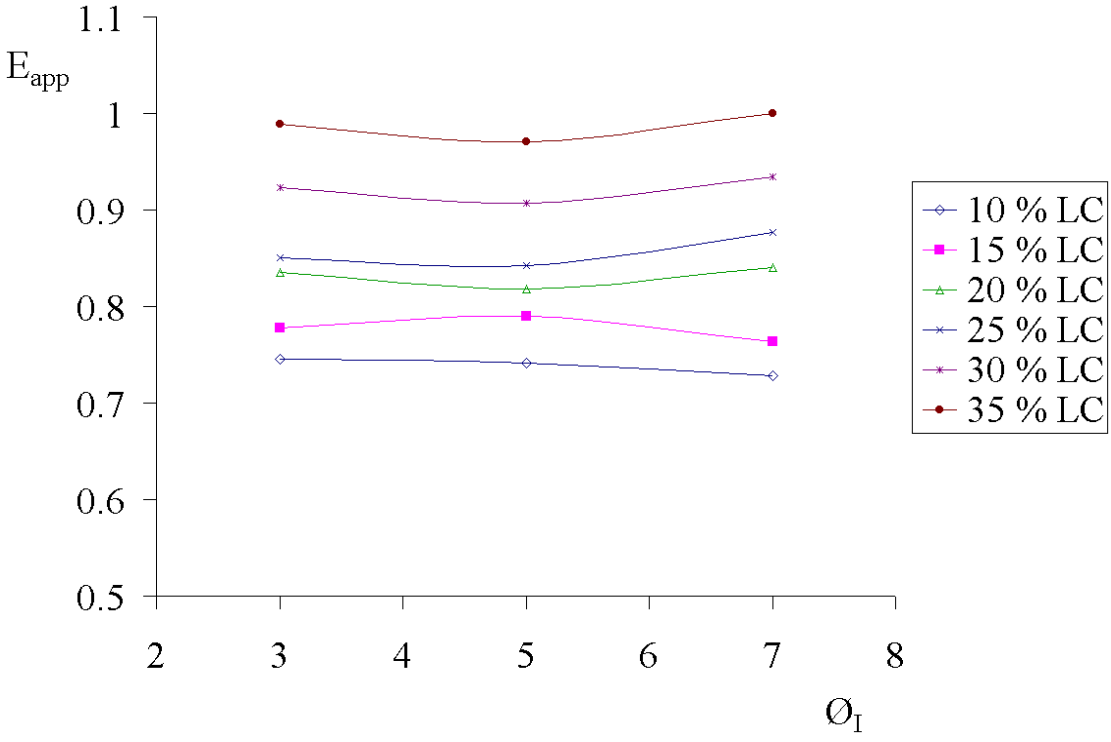

Fig. 15. Effect of the island diameter ($Ø_I$) on the apparent modulus (E_{app}) of the material for varying LC concentrations

6. Concluding remarks

Several competing deformation mechanisms were shown to take place during tensile deformation of the analyzed material. The structure of the material determines which mechanisms can take place, and which are predominant among those, namely:

a) If the chains are highly oriented with the direction of the application of the force, the predominant mechanisms are bond extension and bond conformation change, eventually leading to bond rupture.

b) In the case of coiled chains, additional mechanisms can occur, such chain uncoiling and chain separation, for example through a sliding motion.

c) The magnitudes of the applied force and the deformation speed have also been found to influence, which deformation mechanisms can occur; these results will be published separately.

The presence of physical entanglements in these CGMs allowed the confirmation of their influence on the mechanical response of the material. During deformation, these entanglements can limit the relative motion of the chains and thus contribute to the load-bearing capability of the structure. Experimental results by Goldman [48] and also by Seguela and Rietsch [45] have pointed out the importance of entanglements in the mechanical behavior of polymers.

The simulations show that the rigid LC phase indeed performs its role as reinforcement, increasing the modulus of the material; however, it also favors the formation and propagation of cracks. The material becomes stronger but simultaneously more brittle. Not only the concentration of the second phase is important, but also its distribution in the flexible matrix. In fact, the behavior of materials with random distribution of the LC phase is considerably different from those with very homogenous distributions. Although distributions as those discussed in section 5.5 would not be found in real materials, it becomes clear that poor LC phase dispersion creates regions with higher probability of crack formation and propagation.

Within the studied range, the size of the LC islands was found to have a negligible influence on the mechanical response of the material during most of the deformation process, particularly at the early stages. There is some effect of the island size on the crack formation and propagation patterns, but a more extensive study is required before conclusions can be drawn.

Although the simulations have provided pertinent information about the phenomena occurring at the mesoscale, the jump to macroscopic properties and behavior requires additional work.

Appendix: Simulation model

For performing the simulations, the Newtonian differential equations of motion have been transformed into difference equations, with a finite time step of Δt. The position of the particle at a given moment is calculated with respect to the previous time step after considering the forces acting on the particle, which are calculated by summation of potential interactions and external forces applied on the material. Based on this information, the positions after the next time step are calculated using a leap-frog algorithm [38]. The equations of motion have the form:

$$
\begin{aligned}
x_j^i(t+\Delta t) &= x_j^i(t) + \lambda(t) \times [\, x_j^i(t) - x_j^i(t-\Delta t)\,] + f_j^i x(t) \times (\Delta t)^2 \\
y_j^i(t+\Delta t) &= y_j^i(t) + \lambda(t) \times [\, y_j^i(t) - y_j^i(t-\Delta t)\,] + f_j^i y(t) \times (\Delta t)^2 \\
z_j^i(t+\Delta t) &= z_j^i(t) + \lambda(t) \times [\, z_j^i(t) - z_j^i(t-\Delta t)\,] + f_j^i z(t) \times (\Delta t)^2
\end{aligned}
\qquad (1)
$$

Here, $x_j^i(t)$, $y_j^i(t)$ and $z_j^i(t)$ are the coordinates of the j^{th} segment in the i^{th} chain, $\lambda(t)$ is a kinetic coefficient described below, and $f_j^i x(t)$, $f_j^i y(t)$ and $f_j^i z(t)$ are the forces acting on the segment along each axis.

The simulations were performed at a constant temperature. To consider the effect of thermal forces, a kinetic factor [38] was incorporated into the equations of motion, rescaling the velocity of each particle in each time step by the factor $\lambda(t)$:

$$
\lambda(t) = \left[1 + \left(\frac{U_{k0}}{U_k(t)} - 1 \right) \times \left(\frac{\Delta t}{\tau_T} \right) \right]^{\frac{1}{2}} \qquad (2)
$$

Here, U_{k0} is the reference value of kinetic energy, $U_k(t)$ is the actual value of kinetic energy, and τ_T is the time constant of thermal relaxation. The kinetic energy per particle has been calculated according to the formula:

$$
U_k(t) = \frac{\sum_{i=1}^{n} \sum_{j=1}^{m(i)} \sqrt{[\, x_j^i(t) - x_j^i(t-\Delta t)\,]^2 + [\, y_j^i(t) - y_j^i(t-\Delta t)\,]^2 + [\, z_j^i(t) - z_j^i(t-\Delta t)\,]^2}}{2 \times \Delta t^2 \times \sum_{i=1}^{n} m(i)} \qquad (3)
$$

Here, n is the total number of chains in the material and m(i) is the number of particles in chain i.

In 2D simulations, due to the specific arrangement of the chains, the following formulae were used to calculate the forces acting on the segments along the x axis:

$$
\begin{aligned}
f_j^i(t) = & - \partial U[\, x_{j-1}^i(t) - x_j^i(t)\,] / \partial x_j^i(t) \\
& - \partial U[\, x_{j+1}^i(t) - x_j^i(t)\,] / \partial x_j^i(t) \\
& - \sum_{k=1}^{m(i-1)} \partial U'[\, x_k^{i-1}(t) - x_j^i(t)\,] / \partial x_j^i(t) \\
& - \sum_{l=1}^{m(i+1)} \partial U'[\, x_l^{i+1}(t) - x_j^i(t)\,] / \partial x_j^i(t)
\end{aligned}
\qquad (4)
$$

for $j \neq m(i)$ and $j \neq 1$

$$
\begin{aligned}
f_l^i(t) = & - f_{ext} \\
& - \partial U[\, x_2^i(t) - x_l^i(t)\,] / \partial x_l^i(t) \\
& - \sum_{k=1}^{m(i-1)} \partial U'[\, x_k^{i-1}(t) - x_l^i(t)\,] / \partial x_l^i(t) \\
& - \sum_{l=1}^{m(i+1)} \partial U'[\, x_l^{i+1}(t) - x_l^i(t)\,] / \partial x_l^i(t)
\end{aligned}
\qquad (5)
$$

$$
\begin{aligned}
f^{i}_{m(i)}(t) = f_{ext} & \\
& - \partial U[\, x^{i}_{m(i)-1}(t) - x^{i}_{m(i)}(t)\,] / \partial x^{i}_{m(i)}(t) \\
& - \sum_{k=1}^{m(i-1)} \partial U'[\, x^{i-1}_{k}(t) - x^{i}_{m(i)}(t)\,] / \partial x^{i}_{m(i)}(t) \\
& - \sum_{l=1}^{m(i+1)} \partial U'[\, x^{i+1}_{l}(t) - x^{i}_{m(i)}(t)\,] / \partial x^{i}_{m(i)}(t)
\end{aligned}
\qquad (6)
$$

Here, f_{ext} is the value of the external force applied to the material. In 2D simulations, the external force was always applied to both ends of all chains. Thus, the force on the first and last segments in each chain was calculated differently from all other segments.

In 3D simulations, the forces acting on any segment along each axis can be calculated using the following formulae:

$$
\begin{aligned}
f^{i}_{j}x(t) = f^{i}_{j\,ext}x(t) & - \partial U[\, x^{i}_{j-1}(t) - x^{i}_{j}(t)\,] / \partial x^{i}_{j}(t) \\
& - \partial U[\, x^{i}_{j+1}(t) - x^{i}_{j}(t)\,] / \partial x^{i}_{j}(t) \\
& - \sum_{k=1}^{n}\sum_{l=1}^{m(k)} \partial U'[\, x^{k}_{l}(t) - x^{i}_{j}(t)\,] / \partial x^{i}_{j}(t)
\end{aligned}
\qquad (7)
$$

$$
\begin{aligned}
f^{i}_{j}y(t) = f^{i}_{j\,ext}y(t) & - \partial U[\, y^{i}_{j-1}(t) - y^{i}_{j}(t)\,] / \partial y^{i}_{j}(t) \\
& - \partial U[\, y^{i}_{j+1}(t) - y^{i}_{j}(t)\,] / \partial y^{i}_{j}(t) \\
& - \sum_{k=1}^{n}\sum_{l=1}^{m(k)} \partial U'[\, y^{k}_{l}(t) - y^{i}_{j}(t)\,] / \partial y^{i}_{j}(t)
\end{aligned}
\qquad (8)
$$

$$
\begin{aligned}
f^{i}_{j}z(t) = f^{i}_{j\,ext}z(t) & - \partial U[\, z^{i}_{j-1}(t) - z^{i}_{j}(t)\,] / \partial z^{i}_{j}(t) \\
& - \partial U[\, z^{i}_{j+1}(t) - z^{i}_{j}(t)\,] / \partial z^{i}_{j}(t) \\
& - \sum_{k=1}^{n}\sum_{l=1}^{m(k)} \partial U'[\, z^{k}_{l}(t) - z^{i}_{j}(t)\,] / \partial z^{i}_{j}(t)
\end{aligned}
\qquad (9)
$$

where the following condition applies: $(k \neq i)$ or $(k = i$ and $l \neq j$ and $l \neq j-1$ and $l \neq j+1)$.

Here $f^{i}_{j\,ext}x(t)$ is the component along the x-axis of any external force applied on the j^{th} particle in the i^{th} chain. Likewise, $f^{i}_{j\,ext}y(t)$ and $f^{i}_{j\,ext}z(t)$ are the components along the y-axis and z-axis, respectively.

Acknowledgement: Support for this research has been provided by the Fundação para a Ciência e a Tecnologia, 3° Quadro Comunitário de Apoio, Lisbon, and also by the Robert A. Welch Foundation, Houston (Grant # B-1203).

[1] Samulski, E. T.; *Faraday Disc.* **1985**, *79*, 7.

[2] Mandelkern, L.; Mark, J. E.; Suter, U. W.; Yoon, D. Y.; editors; "*Selected Works of Paul J. Flory*", vol. *3*, Stanford University Press, Stanford, California **1985**.

[3] Flory, P.J.; "*Recent Advances in Liquid Crystalline Polymers*", chap. 6, Chapoy, L. L., editor; Elsevier, London **1985**.

[4] Brostow, W; *Polymer* **1990**, *31*, 979.

[5] Brostow, W; "*Physical Properties of Polymers Handbook*", chap. 33, Mark, J. E., editor; American Institute of Physics Press, Woodbury, New York **1996**.

[6] Hess, M.; Lopez, B. L.; "*Mechanical and Thermophysical Properties of Polymer Liquid Crystals*", chap. 9, Brostow, W., editor; Chapman & Hall, London **1998**.

[7] Brostow, W.; Hibner, K.; Walasek, J.; *J. Chem. Phys.* **1998**, *108*, 6484.

[8] Brostow, W.; Walasek, J.; *J. Chem. Phys.* **2001**, *114*, 2466.

[9] Brostow, W.; D'Souza, N. A.; Kubat, J.; Maksimov, R.; *J. Chem. Phys.* **1999**, *110*, 9706.

[10] Brostow, W.; *Mater. Res. Innovat.* **2000**, *3*, 347.

[11] Akinay, A. E.; Brostow, W.; *Polymer* **2001**, *42*, 4527.

[12] Fossey, S.; "*Performance of Plastics*", p. 63, Brostow, W., editor; Hanser, Munich - Cincinnati **2000**.

[13] Ayyagari, C.; Bedrov, D.; Smith, G. D.; *Macromolecules* **2000**, *33*, 6194.

[14] Gerde, E.; Marder, M.; *Nature* **2001**, *413*, 285.

[15] Karayiannis, N. C.; Mavrantzas, V. G.; Theodorou, D. N.; *Chem. Eng. Sci.* **2001**, *56*, 2789.

[16] Makrodimitris, K.; Papadopoulos, G. K.; Theodorou, D. N.; *J. Phys. Chem. B* **2001**, *105*, 777.

[17] Mavrantzas, V. G.; Theodorou, D. N.; *Macromol. Theory Simul.* **2000**, *9*, 500.

[18] Harmandaris, V. A.; Mavrantzas, V. G.; Theodorou, D. N.; *Macromolecules* **2000**, *33*, 8062.

[19] Andersen, H. C.; *J. Chem. Phys.* **1980**, *72*, 2384.

[20] Banaszak, M.; *TASK Quart.* **2001**, *5*, 17.

[21] Abraham, F. F.; *Phys. Rev. Lett.* **1980**, *44*, 463.

[22] Abraham, F. F.; Rudge, W. E.; Auerbach, D. J.; Koch, S. W.; *Phys. Rev. Lett.* **1984**, *52*, 445.

[23] Fritz, L.; Hofmann, D.; *Polymer* **1997**, *38*, 1035.

[24] Termonia, Y.; "*Encyclopedia of Polymer Science and Technology*", 3rd edition, Wiley-Interscience, New York **2002**.

[25] Termonia, Y.; Smith, P.; *Macromolecules* **1987**, *20*, 835.

[26] Termonia, Y.; Smith, P.; *Macromolecules* **1988**, *21*, 2184.

[27] Termonia, Y.; *Macromolecules* **1994**, *27*, 7378.

[28] Karger-Kocsis, J.; "*Structure Development in Processing for Polymer Property Enhancement*", Cunha, A. M., editor; North Atlantic Treaty Organization, Brussels **1999**.

[29] Santana, O. O.; Maspoch, M. L.; Martinez, A. B.; *Polym. Bull.* **1999**, *39*, 511.

[30] Li, Y.; Ann, H.; Binienda, W. K.; *Internat. J. Solids Structures* **1998**, *11*, 981.

[31] Shbeeb, N.; Binienda, W. K.; Kreider, K.; *Internat. J. Fracture* **2000**, *104*, 23.

[32] Blonski, S.; Brostow, W.; Kubát, J.; *Phys. Rev. B* **1994**, *49*, 6494.

[33] Brostow, W.; Kubát, J.; Kubát, M. J.; *Mech. Compos. Mater.* **1995**, *31*, 432.

[34] Brostow, W.; Hinze, J. A.; Simoes, R.; *J. Mater. Res.* **2004**, *19*, 851.

[35] Brostow, W.; Donahue III, M.; Karashin, C. E.; Simoes, R.; *Mater. Res. Innovat.* **2001**, *4*, 75.

[36] Brostow, W.; Cunha, A. M.; Quintanilla, J.; Simoes, R.; *Macromol. Theory Simul.* **2002**, *11*, 308.

[37] Flory, P. J.; "*Statistical Mechanics of Chain Molecules*", Wiley-Interscience, New York **1969**.

[38] van Gunsteren, W. F.; "*Mathematical Frontiers in Computational Chemical Physics*", Truhlar, D. G., editor; Springer, New York **1988**.

[39] Alder, B. J.; Wainwright, T. E.; *J. Chem. Phys.* **1957**, *27*, 1208.

[40] Rahman, A.; *Phys. Rev.* **1964**, *136*, A405.

[41] Mom, V.; *J. Comput. Chem.* **1981**, *2*, 446.

[42] Brostow, W.; Cunha, A. M.; Simoes, R.; *Mater. Res. Innovat.* **2003**, *7*, 19.

[43] Brostow, W.; Dziemianowicz, T. S.; Romanski, R.; Werber, W.; *Polym. Eng. Sci.* **1988**, *28*, 785.

[44] Brostow, W.; Hibner, K.; Walasek, J.; *Macromol. Theory Simul.* **2001**, *10*, 304.

[45] Seguela, R.; Rietsch, F.; *Polymer* **1986**, *27*, 703.

[46] Brostow, W.; Sterzynski, T.; Triouleyre, S.; *Polymer* **1996**, *37*, 1561.

[47] Brostow, W.; Dziemianowicz, T. S.; Romanski, J.; Werber, W.; *Polym. Eng. Sci.* **1988**, *28*, 785.

[48] Goldman, A. Y.; Venkatashan, K.; *Proc. Ann. Tech. Conf. Soc. Plastics Engrs.* **2002**, *60*, 1363.